NANO EXPRESS

Open Access

Optical Performance of Top-Down Fabricated AlGaN Nanorod Arrays with Multi-Quantum Wells Embedded

Shucheng Ge[1], Jiangping Dai[2], Na Gao[1], Shiqiang Lu[1], Penggang Li[1], Kai Huang[1]* ⓘ, Bin Liu[2]*, Junyong Kang[1], Rong Zhang[1,2] and Youdou Zheng[2]

Abstract

Deep ultraviolet AlGaN-based nanorod (NR) arrays were fabricated by nanoimprint lithography and top-down dry etching techniques from a fully structural LED wafer. Highly ordered periodic structural properties and morphology were confirmed by scanning electron microscopy and transmission electron microscopy. Compared with planar samples, cathodoluminescence measurement revealed that NR samples showed 1.92-fold light extraction efficiency (LEE) enhancement and a 12.2-fold internal quantum efficiency (IQE) enhancement for the emission from multi-quantum wells at approximately 277 nm. The LEE enhancement can be attributed to the well-fabricated nanostructured interface between the air and the epilayers. Moreover, the reduced quantum-confined stark effect accounted for the great enhancement in IQE.

Keywords: DUV AlGaN multi-quantum wells, Nanorod light-emitting diodes, Internal quantum efficiency, Light extraction

Introduction

In the past decade, AlGaN-based UV LEDs have attracted wide attention because of their promising applications such as water purification, sterilization, and biochemical detection. [1–3]. Compared with traditional mercury UV lamps, AlGaN-based UV LEDs are robust, compact, and environmentally friendly and can be turned on without warming up step. However, strong piezoelectric field exists in the AlGaN multi-quantum wells (MQWs), resulting in spatial separation of electrons and holes, named as quantum-confined stark effect (QCSE), which dramatically decreases the internal quantum efficiency (IQE) [4]. Another problem is the low light extraction efficiency (LEE) [5], which is caused not only by the internal total reflection at the epilayers' interface, but also by the dominant transverse magnetic (TM) polarized light [6].
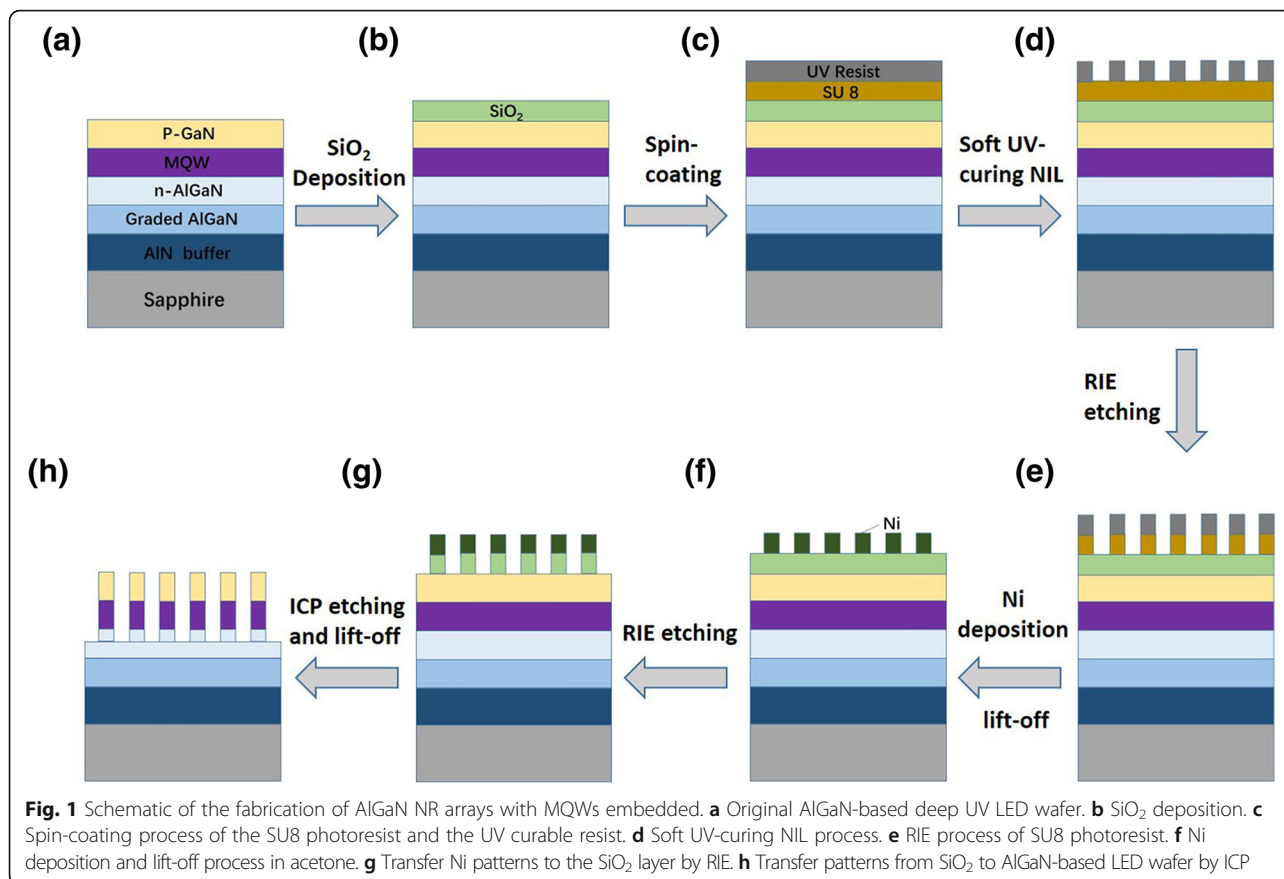
Previous investigations suggested that the energy band engineering is an effective way to reduce the QCSE and thus improve the IQE [7]. On the other hand, the interface engineering, such as incorporating structures like photonic crystal [8, 9], patterned substrate [10, 11], distributed Bragg Reflector [12], and surface plasmons [13–16], can enhance the LEE of the deep UV LEDs. However, the combination of these methods is relatively difficult.

Fabrication of AlGaN-based deep UV nanostructured LEDs can be an alternative way to overcome QCSE and low LEE issues at the same time. Generally, nanostructured LEDs were fabricated by nanometers scale masks and top-down dry etching techniques. The masks were prepared via annealed metal nanoparticles such as nickel (Ni) or gold [17, 18], nanosphere lithography [19–21], electron beam lithography (EBL) [22], and focused ion beam milling [23]. Meanwhile, several selective area epitaxy methods have been developed to obtain InGaN-based nanowire LEDs [24, 25]. However, each method has its own natural disadvantages, such as expensive, uncontrollable morphology, non-uniform, incompatible with microelectronics processes, and time-consuming. In order to overcome these shortcomings, we have

* Correspondence: k_huang@xmu.edu.cn; bliu@nju.edu.cn
[1]Department of Physics, Fujian Key Laboratory of Semiconductor Materials and Applications, Collaborative Innovation Center for Optoelectronic Semiconductors and Efficient Devices, Xiamen University, Xiamen 361005, China
[2]Jiangsu Provincial Key Laboratory of Advanced Photonic and Electronic Materials, School of Electronic Science and Engineering, Nanjing University, Nanjing 210093, China

Ge *et al. Nanoscale Research Letters*   (2019) 14:170

Page 2 of 7

Fig. 1 Schematic of the fabrication of AlGaN NR arrays with MQWs embedded. **a** Original AlGaN-based deep UV LED wafer. **b** SiO$_2$ deposition. **c** Spin-coating process of the SU8 photoresist and the UV curable resist. **d** Soft UV-curing NIL process. **e** RIE process of SU8 photoresist. **f** Ni deposition and lift-off process in acetone. **g** Transfer Ni patterns to the SiO$_2$ layer by RIE. **h** Transfer patterns from SiO$_2$ to AlGaN-based LED wafer by ICP

developed a soft UV-curing nanoimprint lithography (NIL) technique to prepare controllable masks in a very large area, with high uniformity and low density of defects [26, 27].

In this work, we successfully prepared AlGaN nanorod (NR) arrays with MQWs embedded from planar AlGaN LED wafers. Compared with the planar (PLA) samples, 1.92-fold LEE enhancement and 12.2-fold relative IQE enhancement have been demonstrated. Cathodoluminescence (CL), scanning electron microscopy (SEM), and transmission electron microscopy (TEM) measurements suggested that the enhanced LEE can be attributed to the improved interfacial quality between the air and the epilayers. The Raman measurements demonstrated that the strain in the MQWs is reduced from 0.42% to 0.13%, which is beneficial for IQE enhancement.

Methods

The AlGaN LED wafer was grown by metal-organic chemical vapor deposition (MOCVD) on a 2 in. *c* plane sapphire substrate, which is defined as the PLA sample. The epitaxy comprised a 900-nm undoped AlN buffer, a 400-nm graded Al composition AlGaN layer, a 1.4-μm-thick Si-doped n-Al$_{0.5}$Ga$_{0.5}$N, and 5 periods of Al$_{0.35}$Ga$_{0.65}$N/Al$_{0.45}$Ga$_{0.55}$N MQWs with well and barrier

thickness of 3 and 10 nm, respectively, followed by a 100-nm Mg-doped p-GaN contact layer.

A soft UV-curing NIL and a post-growth etching approach have been employed to obtain the AlGaN NR arrays [26–28]. As shown in Fig. 1a–h, NIL process started with a deposition of a 200-nm-thick silicon dioxide (SiO$_2$) by using plasma-enhanced chemical vapor deposition (PECVD) method (Fig. 1b). Then, a layer of 300-nm-thick SU8 photoresist and a layer of 80-nm-thick UV curable resist were directly spin-coated on the epilayer (Fig. 1c), with post soft UV-curing NIL on the UV curable resist (Fig. 1d). To remove the UV resist residue and duplicate the nano-patterns to the SU8 photoresist layer, oxygen (O$_2$) plasma was utilized to etch SU8 photoresist via reactive-ion etching (RIE) procedure (Fig. 1e). After that, a 30-nm-thick Ni layer was deposited via physical vapor deposition (PVD), and lift-off process followed to form periodic Ni islands on the surface of SiO$_2$ layer, which served as the hard mask (Fig. 1f). The prepared Ni hard mask was used to transfer the patterns to SiO$_2$ layer by another RIE process (Fig. 1g). Subsequently, these SiO$_2$ nanorod arrays were employed as a second mask to etch the AlGaN LED wafer via an inductively coupled plasma (ICP) etching process. Finally, these SiO$_2$ nanorod array masks were
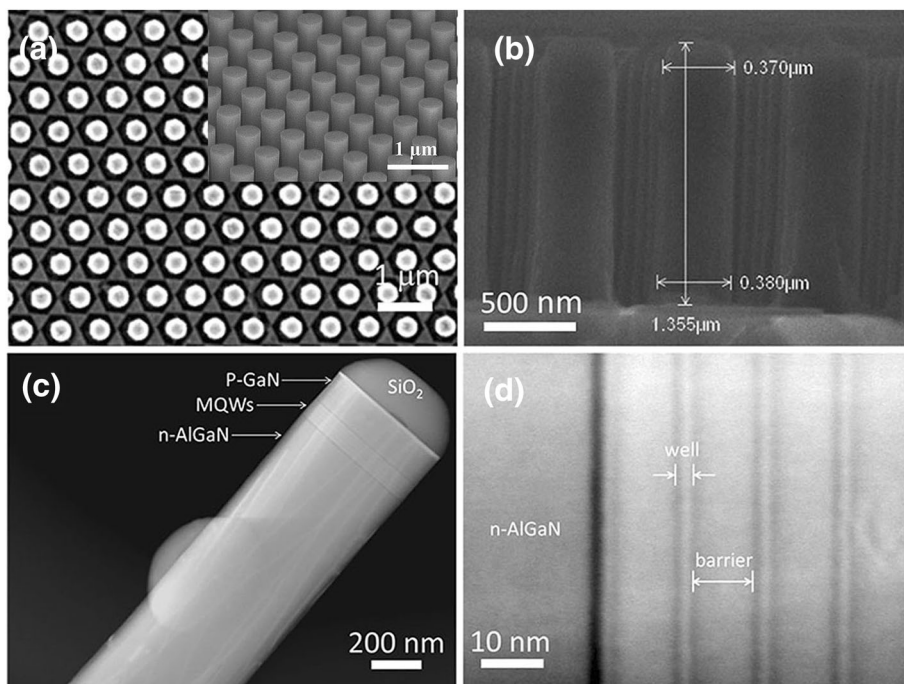
Fig. 2 The top view (**a**), titled (inset in a), and cross-sectional (**b**) SEM images of the AlGaN NR arrays. **c**, **d** the TEM images of single NR and AlGaN MQWs, respectively
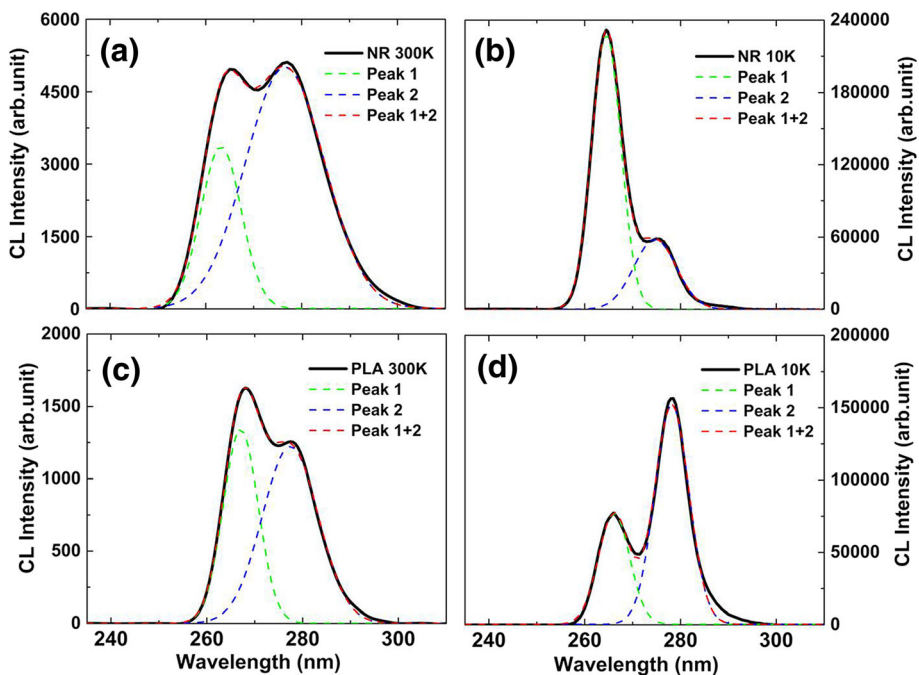

Fig. 3 a, **b** CL spectra of NR samples at 300 K and 10 K, respectively, excited by an electron beam (10 kV, 992 pA). **c**, **d** CL spectra of PLA samples at 300 and 10 K, respectively, excited by an electron beam (10 kV, 992 pA). The solid lines and dash lines are corresponding to the experimental and Gaussian fitting curve

Ge *et al. Nanoscale Research Letters*   (2019) 14:170

Page 4 of 7

removed by HF solution, and AlGaN NR arrays were acquired as depicted in Fig. 1h. The yield of nanostructures with this NIL technology is over 98% on 2 in. wafer, which is comparable with the EBL method but the NIL technology is much cheaper. The details could be found in our previous report [27]. It is inevitable to generate surface states on the sidewall of the nanorods during dry etching, which may serve as non-radiation recombination centers and suppress the luminescence of AlGaN MQWs. Thus, all the NR samples have undergone a chemical treatment by using KOH and dilute acid solution at 90 °C in water bath to remove the surface states.

The morphology of fabricated AlGaN NR arrays was characterized in a ZEISS SIGMA high-resolution field emission SEM system. TEM images were collected by FEI Titan 80-300 TEM system with electron beam operating at 200 kV. The CL spectra were collected by an electron beam-fiber probe system with electron beam operating at 10 kV and 922 pA. The spectra of Raman scattering was obtained in a Confocal Raman spectroscopy imaging system (WITec alpha 300RA) with back-scattering configuration, by using a 514-nm laser as excitation source. The Raman measurement was calibrated by a standard single crystal silicon sample with optical phonon mode at 520.7 cm^{-1}.

Results and Discussion

Figure 2 a, inset in a, and b show the typical top view, titled, and cross-sectional SEM images of the fabricated AlGaN NR arrays with good uniformity and smooth sidewalls. One can see that the NR are in a highly ordered hexagonal array. The diameter, period, and length of the NRs are approximately 350 nm, 730 nm, and 1300 nm, respectively. As shown in Fig. 2 c and d, the MQWs embedded in the NR can be clearly observed after NR fabrication. The well and barrier are presented as dark and bright areas, respectively, and the interface is still legible, flat, and steep.

Figure 3 a and b show the room temperature (RT; 300 K) and low temperature (LT; 10 K) CL spectra of NR samples, respectively. Figure 3 c and d show the RT and LT CL spectra of the PLA samples, respectively. The solid lines and dash lines are experimental and fitted curve

Table 1 The integrated peak intensities of the NR and PLA samples at 300 K and 10 K

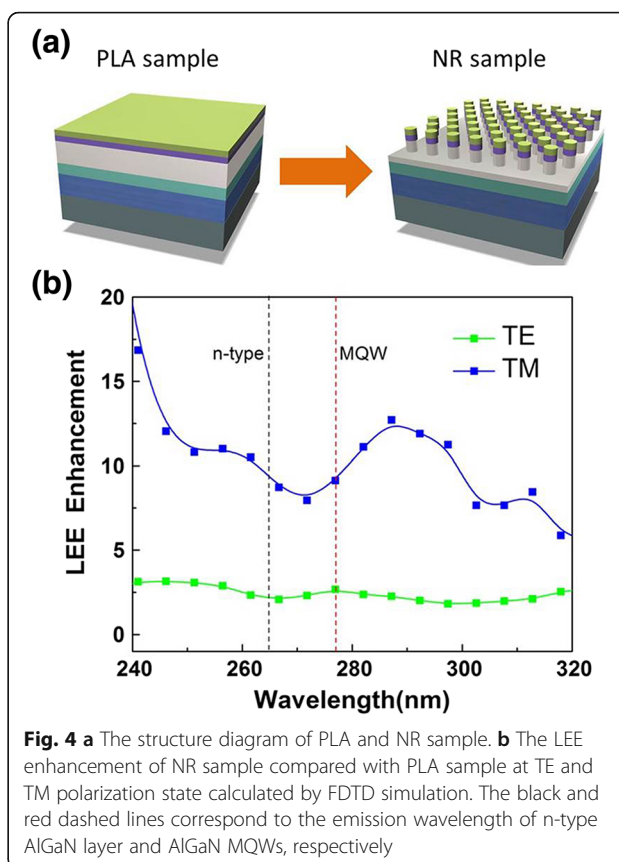|	Peak 1 integrated intensity I_1(a.u.)	Peak 2 integrated intensity I_2(a.u.)
NR 300 K	3.54×10^4	1.04×10^5
NR 10 K	1.74×10^6	6.46×10^5
PLA 300 K	1.23×10^4	1.79×10^4
PLA 10 K	6.27×10^5	1.36×10^6

Fig. 4 a The structure diagram of PLA and NR sample. **b** The LEE enhancement of NR sample compared with PLA sample at TE and TM polarization state calculated by FDTD simulation. The black and red dashed lines correspond to the emission wavelength of n-type AlGaN layer and AlGaN MQWs, respectively

(Gaussian). Gaussian fitting indicates that all spectra consist of two emission peaks. Regardless of the PLA or NR sample, the CL luminescence intensities measured at LT exhibit a great enhancement compared with those under RT. This can be attributed to the weak thermal activation energy at LT. Thus, the carriers cannot migrate to defects where carriers can be non-radiatively recombined, which means that the carriers only perform radiation recombination and the IQE can be regarded as approximately 100%. Considering the structure of the epitaxial layer, the peaks at short (Peak 1) and long (Peak 2) wavelengths are attributed to the emissions of n-type layer and MQW, respectively. The detailed parameters obtained from the Gaussian divided peaks are shown in Table 1. For the NR sample, the integrated intensities of emission from the n-type layer are approximately 2.89 [I_1(NR300K)/ I_1(PLA300K)] and 2.78 [I_1(NR10K)/I_1(PLA10K)] times higher than that for the PLA sample at RT and LT, respectively. However, at RT, the integrated intensity of the emission from the MQW for NR sample is approximately 5.81 [I_2(NR300K)/I_2(PLA300K)] times higher than that of PLA sample, while the ratio is only 0.48 [I_2(NR10K)/I_2(PLA10K)] at LT.

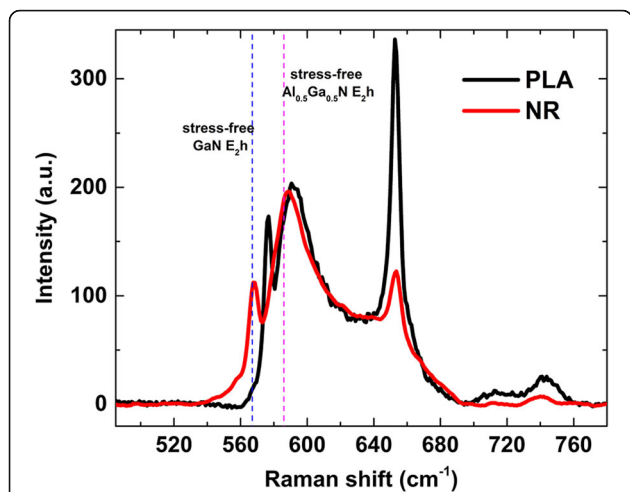Compared with PLA sample, the sidewalls of the NR sample are exposed to the air as shown in Fig. 4a,

Fig. 5 Raman spectra of the PLA and NR samples stimulated by a 514 laser at RT. The black and red curves represent PLA and NR samples, respectively. The blue and pink dashed lines correspond to E_2h peak of unstressed GaN and $Al_{0.5}Ga_{0.5}N$, respectively

resulting in a significant increase of the total interface area between the air and the epilayer. Thus, the LEE can be enhanced for both n-type layer and MQW emissions. The LEE enhancement of the n-type layer emission can be estimated to be approximately 2.8 $[I_1(NR)/I_1(PLA)]$. Moreover, according to the geometric structure obtained from Fig. 2a, the MQW area of the PLA sample is approximately 4 times larger than that of the NR samples. By assuming the IQEs for both PLA and NR samples as 1 at 10 K, the relative light extraction enhancement can be obtained as approximately 1.9 $[4 \times I_2(NR10K)/I_2(PLA10K)]$. Clearly, the LEE enhancement of the n-type layer emission is higher than that of the MQW emission.

Finite-difference time-domain (FDTD) simulations were performed to clarify the LEE enhancement of AlGaN NR arrays. The diameter, period, and length of the NR arrays are set as 350 nm, 730 nm, and 1300 nm, respectively, to accord with the fabricated NR arrays as depicted in Fig. 4a. Other simulation parameters are similar to our previous report [29]. Field collected by monitor was used to integrate the power P_0 that escape from the top surface, and the source power of dipole is defined as P_S, so the LEE is $\eta = P_0/P_S$. And the extraction enhancement can be calculated by $E_n = \eta_r/\eta_p$, where η_p, η_r is the LEE of PLA and NR samples, respectively. Figure 4 b shows the light extraction enhancement of the

NR arrays compared with PLA sample at transverse electric (TE) and TM polarization states. One can see that for the n-type layer emission at approximately 265 nm, the LEE enhancement ratios are approximately 2.4 and 9.2 for the TE and TM polarization states, respectively. Previous investigation indicated that even for compressively grown AlGaN MQWs, strongly TE-polarized emission can be observed at wavelengths as short as 240 nm [30]. Thus, it is reasonable that the LEE enhancement of a mixture of TE and TM states is approximately 2.8. However, the LEE enhancement ratios are approximately 2.6 and 9.1 for the TE and TM polarization state, respectively, at approximately 277 nm. The calculated LEE enhancement ratio of the MQW emission from the experimental data is approximately 1.9, which is smaller than the simulated LEE enhancement ratio of both TE and TM polarization states. This may be attributed to the partly irregular shape of the experimentally fabricated NR arrays shown in Fig. 2a or the re-absorption of the damaged layer caused by the NIL process.

On the other hand, the reduced QCSE can enhance the IQE for the NR sample for the MQW emission. The IQEs of the n-type layer emission at 300 K can be estimated as approximately 1.96% $[I_1(PLA300K)/I_1(PLA10K)]$ and 2.03% $[I_1(NR300K)/I_1(NR10K)]$ for the PLA and NR samples, respectively. They are very close to each other because the QCSE does not exist in the n-type layer. However, the IQEs of the MQW emission at 300 K are approximately 1.32% $[I_2(PLA300K)/I_2(PLA10K)]$ and 16.1% $[I_2(NR300K)/I_2(NR10K)]$ for the PLA and NR samples, respectively. Thus the enhancement ratio of IQE is 12.2 for the MQW emission of the NR sample compared with the PLA sample. This great enhancement of the relative IQE should be attributed to the reduced QCSE of the NR sample. According to some similar works in blue/green LEDs [27, 31], a large strain relaxation due to the NR fabrication will reduce the QCSE effect. The reduced QCSE will increase the wave function overlap of electrons and holes and results in an increased IQE.

Raman measurement was performed to confirm the strain relaxation in the NR samples. Figure 5 shows the Raman spectra of the PLA and NR samples. The E_2(high) phonon mode is usually utilized to characterize the stress state in the epitaxial layers. Notably, three E_2(high) phonon modes are shown in the Raman spectra for both PLA and NR samples, corresponding to the

Table 2 The E_2(high) phonon frequencies (cm^{-1}) observed at 300 K and the calculated stress and strain

	GaN			$Al_{0.5}Ga_{0.5}N$		
	Raman shift (cm^{-1})	Stress (GPa)	Strain	Raman shift (cm^{-1})	Stress (GPa)	Strain
PLA	576.6	− 2.82	− 0.59%	591.3	− 1.63	− 0.34%
NR	568.1	− 0.32	− 0.07%	588.3	− 0.71	− 0.15%

Ge *et al. Nanoscale Research Letters*   (2019) 14:170

Page 6 of 7

GaN contact layer, n-type layer, and AlN buffer layer. Clearly, the peak shifts of PLA and NR samples are different compared with stress-free E_2(high) phonon modes, indicating that the stress state has changed after the PLA sample was fabricated into the NR sample. Usually, the in-plane stress of the epitaxial layers is expressed by the following equation [29]:

$$\omega_{E_2(\text{high})} - \omega_0 = C\sigma, \tag{1}$$

where C is the stress-shift rate ($-3.4 \text{ cm}^{-1}/\text{GPa}$, $-3.1 \text{ cm}^{-1}/\text{GPa}$, and $-3.25 \text{ cm}^{-1}/\text{GPa}$ for GaN, AlN, and $Al_{0.5}Ga_{0.5}N$, respectively) [29]. $\omega_{E_2(\text{high})}$ and ω_0 are the Raman shifts for the E_2(high) mode of the corresponding epitaxial layers in our study and the stress-free materials, respectively. The ω_0 values for GaN and $Al_{0.5}Ga_{0.5}N$ are reported to be 567.0 and 586.0 cm^{-1} at RT, respectively [32]. The strain of the epitaxial layers can be expressed as [33]:

$$\sigma_{xx} = \left[C_{11} + C_{12} - 2\frac{C_{13}^2}{C_{33}} \right] \varepsilon_{xx}, \tag{2}$$

where σ_{xx} is the in-plane stress; ε_{xx} is the in-plane strain, and C_{ij} is the elastic constants of GaN and AlN given in previous report [34], i.e., a proportionality factor of 478.5 GPa for GaN, and 474.5 GPa for $Al_{0.5}Ga_{0.5}N$.

Using Eqs. (1, 2), the Raman shift, stress, and the strain are listed in Table 2. Notably, the strain is greatly reduced in the GaN contact layer. By simply considering a linear interpolation of the strain and stress in the different Al content epilayers, the stress/strain in the MQWs with 35% Al content can be obtained as 1.99 GPa/0.42% and 0.59 GPa/0.13% for the PLA and NR sample, respectively. Thus, a 69% strain has been relaxed in the MQWs layer of the NR sample.

According to previous investigation [35], the polarization field E_w in the quantum wells can be expressed as

$$E_w = \frac{l_b(P_b - P_w)}{l_w\varepsilon_b + l_b\varepsilon_w}, \tag{3}$$

where l_w, l_b, P_w, P_b, and ε_b, ε_w are the widths, total polarizations and dielectric constants of the wells and the barriers, respectively. Thus, not only the piezoelectric polarization but also the spontaneous polarization should be taken into account. The piezoelectric polarization is calculated by $P_{pz} = 2(e_{31} - e_{33}\frac{C_{13}}{C_{33}})\varepsilon_{xx}$ [36], where e_{31}, e_{33}, C_{31}, and C_{33} are obtained by the linear interpolation from the related parameters of GaN and AlN [37, 38], the strain ε_{xx} is calculated by the Raman spectra using linear interpolation method. The spontaneous polarization is obtained by the linear interpolation from the spontaneous polarization of GaN and AlN [37, 39]. Thus, by using the dielectric constant of the wells and the barriers obtained by the linear interpolation from the dielectric constant of GaN

Table 3 Spontaneous polarization, piezoelectric polarization, total polarization, and polarization field in the quantum wells

	Spontaneous polarization (C/m^2)	Piezoelectric polarization (C/m^2)	Total polarization (C/m^2)	Polarization field (C/m^2)
PLA	− 0.0536	0.0066	− 0.047	− 0.00397
NR	− 0.0536	0.002	− 0.0516	− 0.00335

$\varepsilon_{GaN} = 8.9$ and AlN $\varepsilon_{AlN} = 8.5$ [40], the polarization field can be calculated by Eq. (3). Table 3 lists the spontaneous polarization, piezoelectric polarization, total polarization, and polarization field in the quantum wells for PLA and NR samples; one can clearly see that the polarization field is reduced after the NR fabrication.

Conclusion
In summary, highly uniform AlGaN NR arrays with MQWs embedded have been successfully fabricated by NIL and top-down etching techniques. Two peaks corresponding to the emission from the n-type layer (at higher energy) and MQWs (at lower energy) are observed by the CL measurement for both NR and PLA samples at 300 K and 10 K. For the n-type layer emission, an over 2-fold LEE enhancement has been observed while the IQE is hardly enhanced via the NR fabrication. For MQW emission, the LEE enhancement ratio can be estimated around 1.9 and a 12.2-fold IQE enhancement is achieved. Raman spectra demonstrated that the strain is reduced from 0.42% to 0.13% by the NR fabrication, showing a strong evidence of reduced QCSE. Our results indicated that for the samples without great crystal quality, the spatial separation between the electrons and the holes caused by the QCSE would be an important factor for the IQE reduction.

Ge *et al. Nanoscale Research Letters*   (2019) 14:170

Page 7 of 7

Availability of Data and Materials

The datasets generated during and/or analyzed during the current study are available from the corresponding author on request.

Authors' Contributions

SC, NG, SL, and KH designed the experiment and analyzed the data. JD, BL, and RZ explored the NIL technology and made some morphological characterization. PL, SG, KH, and JK participated in the discussions and supervised the writing of the manuscript. All authors read and approved the final manuscript.

Competing Interests

The authors declare that they have no competing interests.

Publisher's Note

Springer Nature remains neutral with regard to jurisdictional claims in published maps and institutional affiliations.

References

1. Taniyasu Y, Kasu M, Makimoto T (2006) An aluminium nitride light-emitting diode with a wavelength of 210 nanometres. Nature 441:325–328
2. Oto T, Banal RG, Kataoka K, Funato M, Kawakami Y (2010) 100 mw deep-ultraviolet emission from aluminium-nitride-based quantum wells pumped by an electron beam. Nat Photonics 4:767–770
3. Chiang YC, Lin BC, Chen KJ, Lin CC, Lee PT, Kuo HC (2014) Enhanced performance of nitride-based ultraviolet vertical-injection light-emitting diodes by non-insulation current blocking layer and textured surface. Nanoscale Res Lett 9:699
4. Cingolani R, Botchkarev A, Tang H, Morkoç H, Traetta G (2000) Spontaneous polarization and piezoelectric field in GaN/Al$_{0.15}$Ga$_{0.85}$N quantum wells: impact on the optical spectra. Phys Rev B 61:2711–2715
5. Takano T, Mino T, Sakai J, Noguchi N, Tsubaki K, Hirayama H (2017) Deep-ultraviolet light-emitting diodes with external quantum efficiency higher than 20% at 275 nm achieved by improving light-extraction efficiency. Appl Phys Express 10:031002
6. Shakya J, Knabe K, Kim KH, Li J, Lin JY, Jiang HX (2005) Polarization of III-nitride blue and ultraviolet light-emitting diodes. Appl Phys Lett 86:3343
7. Kuo YK, Chen FM, Chang JY, Shih YH (2016) Structural design and optimization of near-ultraviolet light-emitting diodes with wide wells. J Appl Phys 119:77
8. Jonathan JR, Wierer J, David A, Megens MM (2009) III-nitride photonic-crystal light-emitting diodes with high extraction efficiency. Nat Photonics 3:163–169
9. Lai F, Yang JF (2013) Enhancement of light output power of GaN-based light-emitting diodes with photonic quasi-crystal patterned on p-GaN surface and n-side sidewall roughing. Nanoscale Res Lett 8:244
10. Bell A, Liu R, Ponce FA, Amano H, Akasaki I, Cherns D (2003) Light emission and microstructure of Mg-doped AlGaN grown on patterned sapphire. Appl Phys Lett 82:349–351
11. Lee CY, Tzou AJ, Lin BC, Lan YP, Chiu CH, Chi GC (2014) Efficiency improvement of GaN-based ultraviolet light-emitting diodes with reactive plasma deposited AlN nucleation layer on patterned sapphire substrate. Nanoscale Res Lett 9:505
12. Nakada N, Nakaji M, Ishikawa H, Egawa T, Umeno M, Jimbo T (2000) Improved characteristics of InGaN multiple-quantum-well light-emitting diode by GaN/AlGaN distributed Bragg reflector grown on sapphire. Appl Phys Lett 76:1804–1806
13. He X, Liu F, Lin F, Shi W (2018) Graphene patterns supported terahertz tunable plasmon induced transparency. Opt Express 26:9931–9944
14. He X, Xiao G, Liu F, Lin F, Shi W (2019) Flexible properties of THz graphene bowtie metamaterials structures. Opt Mater Express 9:44–55
15. He X, Gao P, Shi W (2016) A further comparison of graphene and thin metal layers for plasmonics. Nanoscale 8:10388–10397
16. Gao N, Huang K, Li JC, Li SP, Yang X, Kang JY (2012) Surface-plasmon-enhanced deep-UV light emitting diodes based on AlGaN multi-quantum wells. Sci Rep 2:816
17. Shim JP, Seong WS, Min JH, Kong DJ, Seo DJ, Kim HJ, Lee DS (2016) Size-controlled InGaN/GaN nanorod LEDs with an ITO/graphene transparent layer. Nanotechnology 27:465202
18. Ou Y, Iida D, Fadil A, Ou H (2016) Enhanced emission efficiency of size-controlled InGaN/GaN green nanopillar light-emitting diodes. Int J Opt Photonic Eng l:1
19. Latzel M, Büttner P, Sarau G, Hoflich K, Heilmann M, Chen W (2017) Significant performance enhancement of InGaN/GaN nanorod LEDs with multi-layer graphene transparent electrodes by alumina surface passivation. Nanotechnology 28:055201
20. Hu Y, Hao Z, Lai W, Geng C, Luo Y, Yan Q (2015) Nano-fabrication and related optical properties of InGaN/GaN nanopillars. Nanotechnology 26:075302
21. Dong P, Yan J, Zhang Y, Wang J, Geng C, Zheng H, Wei X (2014) Optical properties of nanopillar AlGaN/GaN MQWs for ultraviolet light-emitting diodes. Opt Express 22:A320–A327
22. Xu X, Qiang W, Li C, Ji Z, Xu M, Yang H, Xu X (2018) Enhanced localisation effect and reduced quantum-confined stark effect of carriers in InGaN/GaN multiple quantum wells embedded in nanopillars. J Lumin 203:216–221
23. Wang Q, Ji Z, Zhou Y, Wang X, Liu B, Xu X (2017) Diameter-dependent photoluminescence properties of strong phase-separated dual-wavelength InGaN/GaN nanopillar LEDs. Appl Surf Sci 410:196–200
24. Al-Khanbashi HA, Almarwani AM (2018) Evaluation of the optical properties of the InGaN/GaN quantum well nanopillar arrays prepared via MOVPE approach. Optik 164:28–35
25. Yamano K, Kishino K (2018) Selective area growth of InGaN-based nanocolumn LED crystals on AlN/Si substrates useful for integrated μ-LED fabrication. Appl Phys Lett 112:091105
26. Zhuang Z, Guo X, Zhang G, Liu B, Zhang R, Zhi T (2013) Large-scale fabrication and luminescence properties of GaN nanostructures by a soft UV-curing nanoimprint lithography. Nanotechnology 24:405303
27. Zhuang Z, Guo X, Liu B, Hu F, Dai JP, Zhang Y (2016) Great enhancement in the excitonic recombination and light extraction of highly ordered InGaN/GaN elliptic nanorod arrays on a wafer scale. Nanotechnology 27:015301
28. Zhuang Z, Li Y, Liu B, Guo X, Dai JP, Zhang G (2015) Optical polarization characteristics of c-plane InGaN/GaN asymmetric nanostructures. J Appl Phys 118:233111
29. Dai JP, Liu B, Zhuang Z, He G, Zhi T, Tao T (2017) Fabrication of AlGaN nanorods with different Al compositions for emission enhancement in UV range. Nanotechnology 28:385205
30. Lin W, Jiang W, Gao N, Cai D, Li S, Kang J (2013) Optical isotropization of anisotropic wurtzite Al-rich AlGaN via asymmetric modulation with ultrathin (GaN)m/(AlN) n superlattices. Laser Photonics Rev 7:572–579
31. Wang Q, Bai J, Gong YP, Wang T (2011) Influence of strain relaxation on the optical properties of InGaN/GaN multiple quantum well nanorods. J Phys D Appl Phys 44:395102
32. Davydov VY, Goncharuk IN, Smirnov AN, Nikolaev AE, Lundin WV (2002) Composition dependence of optical phonon energies and Raman line broadening in hexagonal Al$_x$Ga$_{1-x}$N alloys. Phys Rev B 65:125203
33. Gleize J, Demangeot F, Frandon J, Renucci MA, Widmann F (1999) Phonons in a strained hexagonal GaN–AlN superlattice. Appl Phys Lett 74:703–705
34. Wright AF (1997) Elastic properties of zinc-blende and wurtzite AlN, GaN, and InN. J Appl Phys 82:2833–2839
35. Liu W, Zhu L, Zeng F, Liu B, Feng Z (2013) Influence of GaN barrier thickness on optical properties of in-graded InGaN/GaN multiple quantum wells. Appl Phys Express 6:081001
36. Ambacher O, Foutz B, Smart J, Schaff WJ, Eastman LF (2000) Two dimensional electron gases induced by spontaneous and piezoelectric polarization in undoped and doped AlGaN/GaN heterostructures. J Appl Phys 87:334–344
37. Vurgaftman I, Meyer JR (2003) Band parameters for nitrogen-containing semiconductors. J Appl Phys 94:3676–3696
38. Bernardini F, Fiorentini V, Vanderbilt D (1997) Spontaneous polarization and piezoelectric constants of III-V nitrides. Phys Rev B 56:10024–10027
39. Fiorentini V, Bernardini F, Ambacher O (2002) Evidence for nonlinear macroscopic polarization in III–V nitride alloy heterostructures. Appl Phys Lett 80:1204–1206
40. Wu J (2009) When group-III nitrides go infrared: new properties and perspectives. J Appl Phys 106:011101